The Journal of Chemical Physics

Structure of the electrical double layer at the ice-water interface

Hugh Daigle[1, a)]

Center for Subsurface Energy and the Environment, The University of Texas at Austin, Austin, Texas

(Dated: 11 May 2021)

The surface of ice in contact with water contains sites that undergo deprotonation and protonation, and can act as adsorption sites for aqueous ions. Therefore, an electrical double layer should form at this interface, and existing models for describing the electrical double layer at metal oxide-water interfaces should be able to be modified to describe the surface charge, surface potential, and ionic occupancy at the ice-water interface. I used a surface complexation model along with literature measurements of zeta potential of ice in brines of various strength and pH to constrain equilibrium constants. I then made predictions of ion site occupancy, surface charge density, and partitioning of counterions between the Stern and diffuse layers. The equilibrium constant for cation adsorption is more than 5 orders of magnitude larger than the others constants, indicating that this reaction dominates even at low salinity. Deprotonated OH sites are predicted to be slightly more abundant than dangling O sites, consistent with previous work. Surface charge densities are on the order of ± 0.001 C/m^2 and are always negative at the moderate pH values of interest to atmospheric and geophysical applications (6–9). In this pH range, over 99% of the counterions are contained in the Stern layer. This suggests that diffuse layer polarization will not occur because the ionic concentrations in the diffuse layer are nearly identical to those in the bulk electrolyte, and that electrical conduction and polarization in the Stern layer will be negligible due to reduced ion mobility.

[a)]daigle@austin.utexas.edu

I. INTRODUCTION

Ice occurs in contact with water in many natural systems, including glaciers, permafrost, sea, lake, and river ice, snow, and atmospheric ice crystals[1]. The properties of the ice-water interface, including chemistry and surface forces, control many natural processes like frost heave, glacier motion, sea ice growth, destruction of stratospheric ozone, and possibly charge buildup in thunderstorms[2]. Similarly, ice-water interfacial properties are important for geophysical techniques like electromagnetic surveys, which are used to monitor both permafrost[3–6] and glaciers[7,8]. Of particular importance is understanding adsorption of impurities at the ice-water interface, as this affects surface electrical conductivity[9], premelted layer thickness[10], ice rheology[11], and atmospheric chemical processes including ozone depletion[12–14].

The present work focuses on ice Ih, the hexagonal structure that is stable at ambient conditions[1] and relevant to geophysical and atmospheric applications. The surface chemical structure of pristine ice Ih remains an area of active research due partly to experimental difficulties in probing the surface, and partly to the nature of the surface itself, which may not be homogeneous in terms of atom location and in fact can change over time due to residual entropy[15,16]. As discussed by Petrenko[17], the simple model of Fletcher[18,19] has proven particularly durable in terms of predicting various observed properties of the ice-air interface. In this model, the oxygen atoms at the surface are preferentially oriented with their protons facing out. This should give the surface a net positive charge, and indeed experiments by Petrenko and Colbeck[20] showed that metal and dielectric sliders picked up a positive charge from the surface of pure, polycrystalline ice at temperatures between -5 and -35°C. Dosch et al.[21] similarly demonstrated the presence of a positive surface charge on ice at -12.8°C by measuring the abundance of Bjerrum defects with x-ray diffraction. Although the Fletcher model describes the ice-air interface, it is relevant to the ice-water interface as well due to the existence of a premelted layer at temperatures above about 200 K[22].

However, there are situations in which the ice surface attains a negative surface charge. For instance, in thunderstorms, the surface charge of ice crystals and graupel can be positive or negative depending on temperature, cloud water content, and the presence of airborne impurities like smoke[23–25]. This is not necessarily inconsistent with the Fletcher model. Pedersen et al.[26] used long-timescale kinetic Monte Carlo simulations to show that molecular

reordering can occur on the basal plane of ice Ih, which might suggest that even pure ice does not always have a positive surface charge. Dash et al.[27] showed that the rate of ice crystal growth can also influence the surface charge when ice is grown from vapor, as in thunderstorms. In particular, when crystal growth occurs at a sufficiently large free energy difference between the liquid or vapor phase and the solid phase (above the so-called roughening transition), the ice surface is rough and disordered, with OH^- ions preferentially present at asperities[2,27]. The presence of a thin premelted film of water between ice and negatively charged silicate minerals typical of soils also points to a negative surface charge on the ice since the existence of the premelted film relies on a balance between attractive van der Waals forces and repulsive electrostatic forces[2,28]. Finally, when a thin premelted layer separates the bulk ice from air, the charge on the ice-water interface may be affected by protonation and deprotonation reactions on the nearby air-water interface, which assumes a negative charge at pH greater than about 4[29,30]. Zeta potential measurements of the interface between bulk ice and bulk water phases have demonstrated that the interface always has a negative charge at neutral pH[31–35].

Dangling valences in the form of H and O atoms and are known to exist on the ice surface from theoretical computation and experimental observation[36–42]. As Buch et al.[39] note, these dangling valences provide important surface sites for adsorbates. When the ice surface is in contact with water containing dissolved ions, the ions will be attracted to unbalanced charges at the ice-water interface, resulting in the formation of an electrical double layer. Petrenko and Ryzhkin[43] theoretically predicted the existence of an electrical double layer on the surface of pure ice whose thickness corresponded roughly to the thickness of the premelted layer. Kallay et al.[44] and Inagawa et al.[35] showed that the zeta potential of the ice surface in contact with brines could be described with the Guoy-Chapman model for the electrical double layer in a manner analogous to metal oxide-brine interfaces. While previous work has analyzed surface charge and electrical conduction at the ice-water interface, the links between surface reactions with the charge and more importantly the structure of the electrical double layer has not been presented. Here, I extend an existing model for surface reactions at the ice-water interface, compare the model with data from the literature, and make some predictions of charge distribution within the electrical double layer.

II. SURFACE REACTION AND CHARGE MODEL

A. Model development

In hexagonal ice Ih, water molecules are arranged in a tetrahedral lattice in which most of the lattice energy comes from hydrogen bonds[1]. The arrangement of atoms in the ice lattice should conform to the Bernal-Fowler-Pauling ice rules, which state that (1) every oxygen atom is bonded covalently to 2 hydrogen atoms, and (2) every O–O vertex contains 1 hydrogen atom[15,45]. These rules are sometimes violated, resulting in point defects. Ionic defects arise from violations of the first rule, resulting in the presence of H_3O^+ or OH^- ions. Bjerrum defects are the result of violating the second rule, with L- and D-defects corresponding to O–O vertices with 0 or 2 hydrogen atoms[1,46]. On the surface of an ice crystal, the first rule is violated because of a lack of available bonds[47], so the surface has dangling H and O atoms[36,39]. The ordering and spatial arrangement of these dangling bonds on pristine ice surfaces is an area of active research (e.g.,[39,40,47,48].

In the present work, I am concerned with reactions that occur on the surface of ice in equilibrium with a bulk aqueous phase. This situation arises in many natural systems, including saline permafrost and glaciers and snow that are close enough to the melting point to have an interconnected network of premelted layers through a polycrystalline structure. At a molecular level, the ice-water interface is not a discrete interface but a zone about 1 nm thick across which the molecular ordering changes from that of crystalline ice to liquid water[49–51]. The behavior of ions at this interface has been investigated in a few studies[42,51,52], which have demonstrated that Na^+ cations exhibit a strong affinity for the ice-water interface through interactions with O atoms, while anions, particularly Cl^- and F^-, tend to bind with positively charged dangling H^+ atoms and can also penetrate into the ice crystal lattice by replacing O atoms and creating Bjerrum L-defects[1,53,54]. Because the ice-water interface is the interface between a solid and its melt, ionic association occurs not on a 2-dimensional surface but on a surface where the ions can penetrate at least partially into the surface. This has been demonstrated through molecular dynamics simulations both of salt ions[42,51,52] and metal cations[55]. In the limit of complete penetration of the interface by dissolved ions, no charge separation between the aqueous phase and the ice surface can exist, and the surface would lack a zeta (electrokinetic) potential[56]. The presence of a measurable zeta potential,

and its variation with salinity and pH, suggests that the ice-water interface can be treated as a quasi-2-dimensional surface insofar as ionic association and electrical charge are concerned.

The amphoteric nature of water suggests that the dangling H and O atoms on the ice surface can undergo protonation and deprotonation in equilibrium with an aqueous phase, and further can act as Lewis acids and bases and serve as sorption sites for dissolved ions. In light of this, it should be expected that surface reactions at the ice-water interface can be described in a manner analogous to existing models for metal oxides in aqueous solutions. Kallay et al.[44] and Inagawa et al.[35] both demonstrated that such models could explain the variation of zeta potential at the ice-water interface as a function of salinity and pH. Here I show the development of such a model to describe the distribution of charge within the electrical double layer at the ice-water interface. I consider six reactions: protonation and deprotonation of surface hydroxyls, sorption of H^+ and dissolved cations on dangling O atoms, and adsorption and desorption of dissolved ions at charged surface sites. Water molecules in the ice crystal structure at the ice-water interface can be oriented either with a hydrogen atom or a lone pair pointing towards the water phase. The dangling hydrogen atoms can undergo protonation or deprotonation. Following Schindler and Stumm[57], the protonation and deprotonation reactions are

$$\text{—OH} + \text{H}^+ \leftrightarrow \text{—OH}_2^+, \tag{1}$$

$$\text{—OH} \leftrightarrow \text{—O}^- + \text{H}^+, \tag{2}$$

with equilibrium constants K_p and K_d. The deprotonated and protonation sites can act as sorption sites for dissolved ions in the aqueous phase. Considering a simple 1:1 electrolyte, the ion association reactions on deprotonated and protonated sites are

$$\text{—O}^- + \text{C}^+ \leftrightarrow \text{—OC}, \tag{3}$$

$$\text{—OH}_2^+ + \text{A}^- \leftrightarrow \text{—OH}_2\text{A}, \tag{4}$$

where C^+ and A^- represent the electrolyte cations and anions. The equilibrium constants for Eqs. 3 and 4 are K_C and K_A. Water molecules at the ice-water interface oriented with lone pairs on oxygen atoms pointing toward the liquid phase represent negatively charged surface

sites that can adsorb H^+ and C^+ ions. Assuming that these oxygen atoms are hydrogen-bonded to one H atom of a neighboring water molecule in the ice lattice, these sites have a single negative charge and the ion association reactions are

$$> \mathrm{O{+}H^+} \longleftrightarrow \mathrm{—OH}, \tag{5}$$

$$> \mathrm{O{+}C^+} \longleftrightarrow \mathrm{—OC}, \tag{6}$$

with equilibrium constants K_{HO} and K_{CO}.

The reactions in Eqs. 3, 4, and 6 represent surface charge neutralization, and the ions involved are referred to as counterions. The interaction of counterions with the ice surface gives rise to an electrical double layer: the Stern layer, which contains the counterions, and the diffuse layer, within which the ionic concentrations vary with distance from their concentration at the Stern plane to their concentrations in the bulk electrolyte (Fig. 1). For simplicity, I assume that the Stern layer is immediately adjacent to the ice-water interface and ignore any possible counterion penetration into the ice surface. Such penetration would increase the capacitance of the Stern layer and result in a smaller potential difference between the ice-water interface and the Stern plane[56]. However, since the degree of penetration, if any, is difficult to constrain, I will proceed with the understanding that Stern layer capacitances may be underestimated from this model. In the model of Grahame[58], the Stern layer is divided into the inner and outer Helmholtz layers by the β plane, which is located along the centers of cations or anions that are adsorbed directly to the ice surface. Hydrated ions do not approach the surface as closely, and the Stern plane is located along the centers of hydrated ions that associate with the surface.

Following Revil and Glover[59], the equilibrium conditions for Eqs. 1–6 are expressed in terms of electrochemical potentials μ_i^0 as

$$\mu^0_{s,\mathrm{OH}} + \mu^0_{\mathrm{H^+}} = \mu^0_{s,\mathrm{OH_2^+}}, \tag{7}$$

$$\mu^0_{s,\mathrm{OH}} = \mu^0_{s,\mathrm{O^-}} + \mu^0_{\mathrm{H^+}}, \tag{8}$$

$$\mu^0_{s,\mathrm{O^-}} + \mu^0_{\mathrm{C^+}} = \mu^0_{s,\mathrm{OC}}, \tag{9}$$

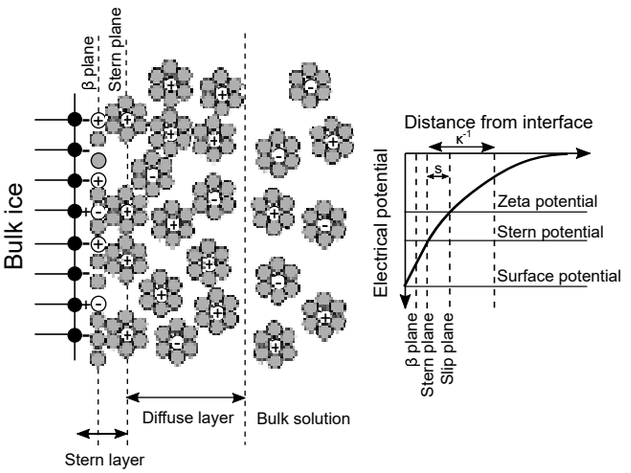

FIG. 1. Electrical double layer at the ice-water interface. Left: configuration of the Stern and diffuse layers at moderate pH. The Stern and β planes are labeled. O atoms on the ice surface (black circles) are protonated or deprotonated, and counterions (white circles) are arranged in the Stern layer where they neutralize the unbalanced charge. Gray circles represent water molecules at the ice surface and as hydration shells around aqueous ions. Right: electrical potential as a function of distance from the ice-water interface with important potentials noted. From the Debye-Hückel approximation, the Debye length κ^{-1} is the length over which the potential decreases by a factor of 1/e from its value at the Stern plane and the diffuse layer extends a distance $2\kappa^{-1}$ from the Stern plane.

$$\mu^0_{s,\mathrm{OH_2^+}} + \mu^0_{\mathrm{A^-}} = \mu^0_{s,\mathrm{OH_2A}}, \tag{10}$$

$$\mu^0_{s,>\mathrm{O}} + \mu^0_{\mathrm{H^+}} = \mu^0_{s,\mathrm{OH}}, \tag{11}$$

$$\mu^0_{s,>\mathrm{O}} + \mu^0_{\mathrm{C^+}} = \mu^0_{s,\mathrm{OC}}, \tag{12}$$

where the subscript s denotes a surface site (all nomenclature is defined in Table 1). The electrochemical potentials are related to the standard chemical potentials by $\mu_i^0 = \mu_i^{(\circ)} + kT \ln \Gamma_i^0$ for surface sites, where Γ_i^0 is the number density of surface site species i; and $\mu_i^0 = \mu_i^{(\circ)} + kT \ln 1000 N_A a_i - e z_i \varphi_\beta$ for ions in solution and $\mu_i^0 = \mu_i^{(\circ)} + kT \ln 1000 N_A a_i - e z_i \varphi_0$ for $\mathrm{H^+}$, where a_i is the activity of ionic species i in the bulk aqueous phase, N_A is Avogadro's

number, e is the elementary charge, z_i is the charge number of the ion (positive or negative), φ_0 is the surface potential, and φ_β is the potential on the β plane. Here, surface sites are defined as dangling OH and O associated with water molecules in the outermost layer of the ordered structure of ice. In the case of surface sites, the difference between the electrochemical and standard chemical potentials is due to the entropy associated with the different arrangements of the surface sites, while in the case of ions the difference is due to entropy as well as the change in potential energy that results from bringing the ion from a reference state at infinite distance to the surface.

Variable	**Description**	**Dimensions**
A	Debye-Hückel function A	$(\mathrm{M/mol})^{\frac{1}{2}}$
a	Debye-Hc̈kel constant	L
a_i	Activity of species i	$\mathrm{mol/L^3}$
B	Debye-Hückel function B	$(1/\mathrm{L})(\mathrm{M/mol})^{\frac{1}{2}}$
b	Debye-Hückel constant	$\mathrm{L^3/mol}$
C	Stern layer capacitance	$\mathrm{T^4I^2/ML^2}$
C_f	Molar concentration of electrolyte in bulk aqueous phase	$\mathrm{mol/L^3}$
C_i^f	Molar concentration of ionic species i in bulk aquous phase	$\mathrm{mol/L^3}$
e	Elementary charge	$\mathrm{M^{\frac{1}{2}}L^{\frac{3}{2}}T}$
f	Counterion partition coefficient	-
I	Ionic strength	$\mathrm{mol/L^3}$
I_m	Ionic strength in molality	mol/M
k	Boltzmann's constant	$\mathrm{ML^2/T^2\theta}$
K_A	Equilibrium constant for anion sorption on protonated sites	-
K_C	Equilibrium constant for cation sorption on deprotonated sites	-
K_{CO}	Equilibrium constant for cation sorption on dangling O	-
K_d	Equilibrium constant for deprotonation	-

K_{HO}	Equilibrium constant for H^+ sorption on dangling O	-
K_p	Equilibrium constant for protonation	-
N_A	Avogadro's number	1/mol
pK_w	Water dissociation constant	-
Q_s	Charge density in the diffuse layer	$M^{\frac{1}{2}}/L^{\frac{1}{2}}T$
Q_s^0	Surface charge density	$M^{\frac{1}{2}}/L^{\frac{1}{2}}T$
R	Universal gas constant	$ML^2/^2mol$
T	Temperature	θ
z_i	Charge number of ionic species i	$1/L^2$
α	Inverse surface site density of OH groups	-
γ_i	Activity coefficient	-
Γ_i^0	Number density of surface site species i	$1/L^2$
Γ_i^d	Equivalent surface site density of species i in the diffuse layer	$1/L^2$
Γ_s^0	Total surface site density	$1/L^2$
ε	Relative dielectric permittivity	-
ε_0	Vacuum dielectric permittivity	L/L
ε_w	Water relative dielectric permittivity	-
ζ	Zeta potential	$M^{\frac{1}{2}}L^{\frac{1}{2}}T$
κ	Inverse Debye length	1/L
$\mu_i^{(\circ)}$	Standard chemical potential of species i	ML^2/T^2
μ_i^0	Electrochemical potential of species i	ML^2/T^2
ρ	Water density	M/L^3
φ	Potential	$M^{\frac{1}{2}}L^{\frac{1}{2}}T$
$\widetilde{\varphi}_d$	Dimensionless reduced Stern potential	-
φ_0	Surface potential	$M^{\frac{1}{2}}L^{\frac{1}{2}}T$
φ_d	Stern potential	$M^{\frac{1}{2}}L^{\frac{1}{2}}T$
φ_β	Potential on the β-plane	$M^{\frac{1}{2}}L^{\frac{1}{2}}T$

Ω_i^0	Fractional surface site occupancy of species i	-

TABLE I: Nomenclature

The equilibrium constants are defined in terms of the standard chemical potentials of the species involved in Eqs. 1–6:

$$\ln K_p = \frac{1}{kT}(\mu^{(\circ)}_{\mathrm{OH}} + \mu^{(\circ)}_{\mathrm{H^+}} - \mu^{(\circ)}_{\mathrm{OH_2^+}}), \tag{13}$$

$$\ln K_d = \frac{1}{kT}(\mu^{(\circ)}_{\mathrm{OH}} - \mu^{(\circ)}_{\mathrm{O^-}} - \mu^{(\circ)}_{\mathrm{H^+}}), \tag{14}$$

$$\ln K_C = \frac{1}{kT}(\mu^{(\circ)}_{\mathrm{O^-}} + \mu^{(\circ)}_{\mathrm{C^+}} - \mu^{(\circ)}_{\mathrm{OC}}), \tag{15}$$

$$\ln K_A = \frac{1}{kT}(\mu^{(\circ)}_{\mathrm{OH_2^+}} + \mu^{(\circ)}_{\mathrm{A^-}} - \mu^{(\circ)}_{\mathrm{OH_2A}}), \tag{16}$$

$$\ln K_{HO} = \frac{1}{kT}(\mu^{(\circ)}_{\mathrm{>O}} + \mu^{(\circ)}_{\mathrm{H^+}} - \mu^{(\circ)}_{\mathrm{OH}}), \tag{17}$$

$$\ln K_{CO} = \frac{1}{kT}(\mu^{(\circ)}_{\mathrm{>O}} + \mu^{(\circ)}_{\mathrm{C^+}} - \mu^{(\circ)}_{\mathrm{OC}}), \tag{18}$$

where k is Boltmann's constant, T is absolute temperature, and $\mu_i^{(\circ)}$ is the standard chemical potential of species i.

Combining these relationships with Eqs. 7–12 yields

$$K_p = \frac{\Gamma^0_{\mathrm{OH_2^+}}}{\Gamma^0_{\mathrm{OH}} a_{\mathrm{H^+}}} \mathrm{e}^{\frac{e\varphi_0}{kT}}, \tag{19}$$

$$K_d = \frac{\Gamma^0_{\mathrm{O^-}} a_{\mathrm{H^+}}}{\Gamma^0_{\mathrm{OH}}} \mathrm{e}^{-\frac{e\varphi_0}{kT}}, \tag{20}$$

$$K_C = \frac{\Gamma^0_{\mathrm{OC}}}{\Gamma^0_{\mathrm{O^-}} a_{\mathrm{C^+}}} \mathrm{e}^{\frac{e\varphi_\beta}{kT}}, \tag{21}$$

$$K_A = \frac{\Gamma^0_{\mathrm{OH_2A}}}{\Gamma^0_{\mathrm{OH_2^+}} a_{\mathrm{A^-}}} \mathrm{e}^{-\frac{e\varphi_\beta}{kT}}, \tag{22}$$

$$K_{HO} = \frac{\Gamma^0_{\mathrm{OH}}}{\Gamma^0_{>\mathrm{O}} a_{\mathrm{H}^+}} \mathrm{e}^{\frac{e\varphi_0}{kT}}, \tag{23}$$

$$K_{CO} = \frac{\Gamma^0_{\mathrm{OC}}}{\Gamma^0_{>\mathrm{O}} a_{\mathrm{C}^+}} \mathrm{e}^{\frac{e\varphi_\beta}{kT}}. \tag{24}$$

It should be noted that only 5 of these constants are independent because no distinction is made between surface OH and OC sites formed by association with deprotonated hydroxyls and dangling O atoms. Therefore,

$$K_{CO} = K_d K_C K_{HO}. \tag{25}$$

The surface charge density Q^0_s is simply the sum of the charge densities of each surface site:

$$Q^0_s = \sum_{i=1} e z_i \Gamma^0_i. \tag{26}$$

Since $z = 0$ for the neutral surface sites,

$$Q^0_s = e(\Gamma^0_{\mathrm{OH}^+_2} - \Gamma^0_{\mathrm{O}^-} - \Gamma^0_{>\mathrm{O}}). \tag{27}$$

Let the fractional surface site occupancies for positive sites Ω^0_+ and for negative sites Ω^0_- be defined as

$$\Omega^0_+ = \frac{\Gamma^0_{\mathrm{OH}^+_2}}{\Gamma^0_s} = \frac{\Gamma^0_{\mathrm{OH}} a_{\mathrm{H}^+} K_p}{\Gamma^0_s} \mathrm{e}^{-\frac{e\varphi_0}{kT}}, \tag{28}$$

$$\Omega^0_- = \frac{\Gamma^0_{\mathrm{O}^-} + \Gamma^0_{>\mathrm{O}}}{\Gamma^0_s} = \frac{\Gamma^0_{\mathrm{OH}}}{\Gamma^0_s a_{\mathrm{H}^+}} (K_d + \frac{1}{K_{HO}}) \mathrm{e}^{\frac{e\varphi_0}{kT}}, \tag{29}$$

where the total surface site density Γ^0_s is

$$\Gamma^0_s = \Gamma^0_{\mathrm{OH}} + \Gamma^0_{\mathrm{OH}^+_2} + \Gamma^0_{\mathrm{O}^-} + \Gamma^0_{>\mathrm{O}} + \Gamma^0_{\mathrm{OC}} + \Gamma^0_{\mathrm{OH_2A}}. \tag{30}$$

From Eqs. 19–25 and 30, the ratio $\frac{\Gamma^0_s}{\Gamma^0_{\mathrm{OH}}}$ can be expressed as

$$\frac{\Gamma^0_s}{\Gamma^0_{\mathrm{OH}}} = 1 + \left[K_d + \frac{1}{K_{HO}} + \frac{K_{CO} a_{\mathrm{C}^+}}{K_{HO}} \mathrm{e}^{-\frac{e\varphi_\beta}{kT}} \right] \frac{\mathrm{e}^{\frac{e\varphi_0}{kT}}}{a_{\mathrm{H}^+}} + \left[1 + K_A a_{\mathrm{A}^-} \mathrm{e}^{\frac{e\varphi_\beta}{kT}} \right] K_p a_{\mathrm{H}^+} \mathrm{e}^{-\frac{e\varphi_0}{kT}} = \alpha. \tag{31}$$

Combining Eq. 31 with Eqs. 28 and 29 yields

$$\Omega_+^0 = \frac{a_{\mathrm{H}^+} K_p}{\alpha} \mathrm{e}^{-\frac{e\varphi_0}{kT}}, \tag{32}$$

$$\Omega_-^0 = \frac{1}{\alpha a_{\mathrm{H}^+}} (K_d + \frac{1}{K_{HO}}) \mathrm{e}^{\frac{e\varphi_0}{kT}}, \tag{33}$$

so Eq. 27 becomes

$$Q_s^0 = e\Gamma_s^0(\Omega_+^0 - \Omega_-^0) = \frac{e\Gamma_s^0}{\alpha}(a_{\mathrm{H}^+} K_p \mathrm{e}^{-\frac{e\varphi_0}{kT}} - \frac{K_d + \frac{1}{K_{HO}}}{a_{\mathrm{H}^+}} \mathrm{e}^{\frac{e\varphi_0}{kT}}). \tag{34}$$

Electroneutrality requires that the surface charge be balanced by the charge in the diffuse layer Q_s such that $Q_s^0 + Q_s = 0$. Assuming the Debye-Hückel approximation of low surface potential (expressed for a 1:1 electrolyte as $|\frac{e\varphi_d}{2kT}| \ll 1$, where φ_d is the potential at the Stern plane), from Pride[60] and Revil and Glover[59] Q_s may be expressed as

$$Q_s = 2000\kappa^{-1} \sum_{i=1} e z_i N_A C_i^f \mathrm{e}^{\frac{z_i \widetilde{\varphi}_d}{2}}, \tag{35}$$

where $\widetilde{\varphi}_d = -\frac{e\varphi_d}{kT}$ is the dimensionless reduced Stern potential and κ^{-1} is the Debye length given by

$$\kappa^{-1} = \sqrt{\frac{\varepsilon\varepsilon_0 kT}{2000 N_A e^2 I}}, \tag{36}$$

where ε is the relative dielectric permittivity of the electrolyte, ε_0 is the vacuum permittivity, and I is the ionic strength in mol/l. While the Debye-Hückel approximation is strictly valid for $|\varphi_d| \ll 47$ mV at $T = 0$°C, Pride[60] suggested it could be valid at even larger potentials, though the upper limit is not defined. Available data in the literature suggest that $|\varphi_d| < 47$ mV at the ice-water interface[33,35,44], so the Debye-Hückel approximation is probaby valid here.

Eqs. 35 and 36 may be combined with the electroneutrality condition for the electrolyte ($C_{\mathrm{A}}^f + C_{\mathrm{OH}^-}^f = C_{\mathrm{C}}^f + C_{\mathrm{H}^+}^f$), where C_i^f is the molar concentration of species i in the aqueous phase, to arrive at the Grahame equation in terms of salinity and pH[44,59]:

$$Q_s = \sqrt{8000\varepsilon\varepsilon_0 kT N_A I} \sinh \frac{\widetilde{\varphi}_d}{2}, \tag{37}$$

where C_f is the electrolyte concentration in mol/l. Assuming that changes in pH are brought about by the addition of either HA or COH, where again A stands for a monovalent anion and C stands for a monovalent cation, let $C^f_{\mathrm{H^+}} = 10^{-\mathrm{pH}} = C_{acid}$ and $C^f_{\mathrm{OH^-}} = 10^{\mathrm{pH}\mathrm{pK_w}} = C_{base}$ where $\mathrm{pK_w}$ is the dissociation constant for water (13.8). Under acidic conditions $C_f = C^f_{\mathrm{C}}$ and $C^f_{\mathrm{A}} = C_f + C_{acid}$. while under basic conditions $C^f_{\mathrm{A}} = C_f$ and $C^f_{\mathrm{C}} = C_f + C_{base}$. Combining Eqs. 34 and 37, the behavior of the surface and Stern potentials as a function of pH, salinity, and temperature is described by

$$\sqrt{8000\varepsilon\varepsilon_0 kTN_A I}\sinh\frac{\widetilde{\varphi}_d}{2} + \frac{e\Gamma^0_s}{\alpha}(a_{\mathrm{H^+}}K_p\mathrm{e}^{-\frac{e\varphi_0}{kT}} - \frac{K_d + \frac{1}{K_{HO}}}{a_{\mathrm{H^+}}}\mathrm{e}^{\frac{e\varphi_0}{kT}}) = 0. \tag{38}$$

B. Method of solution

The potentials and equilibrium constants in Eq. 38 can be determined through comparison with laboratory data. Typically what is known in laboratory measurements is pH, salinity, temperature, and zeta potential. The zeta potential ζ is the potential at the slip plane, which is located within the diffuse layer some distance from the Stern plane (Fig. 1). Estimates of this distance vary: Kallay et al.[44] assumed a value of 15 Å, which they selected based on previous work on adsorption of alcohols and organic molecules on hematite[61,62]. Revil and Glover[59] found a vlue of 2.4 Å for quartz in contact with KCl solution based on a fit of experimental data. Other studies assume that the slip plane coincides with the Stern plane[60,63], which is probably reasonable in the absence of macromolecule or polymer adsorption[64]. Therefore I assumed that $\zeta = \varphi_d$. Next, I assumed following Kallay et al.[44] that the β- and Stern planes are collocated and that $\varphi_\beta = \varphi_d$. This is consistent with the reactions in Eqs. 1–4 in which only electrostatic interactions are assumed between electrolyte ions and the ice surface and there is no specific adsorption[65]. In this case, the capacitance C of the Stern layer is

$$C = \frac{Q^0_s}{\varphi_0 - \varphi_d}. \tag{39}$$

I assumed $C = 1$ F/m^2, which is consistent with estimates from metal oxide-water interfaces[66,67].

The activities of ions in solution are determined from the molar concentrations C^f_i as $a_i = \gamma_i C^f_i$, where γ_i is the activity coefficient. The activity coefficient is calculated from

Debye-Hückel theory extended to high salinity[68]:

$$\log_{10}\gamma_i = -\frac{Az_i^2\sqrt{I_m}}{1+Ba\sqrt{I_m}} + bI_m, \tag{40}$$

where I_m is the ionic strength in molality and a and b are constants. The functions A and B are given by

$$A = \frac{N_A^2 e^3\sqrt{2\rho}}{8\pi \ln 10(\varepsilon_w\varepsilon_0 RT)^{\frac{3}{2}}}, \tag{41}$$

$$B = \frac{N_A e\sqrt{2\rho}}{\sqrt{\varepsilon_w\varepsilon_0 RT}}, \tag{42}$$

where R is the universal gas constant and ρ and ε_w are the density and relative dielectric permittivity of water. Eq. 40 is valid up to ionic strengths of about 2 molal or slightly less than 2000 mM for NaCl and HCl[69]. Here, for simplicity I assumed $\rho = 1000$ kg/m^3, and used $a = 4.78$ Å and $b = 0.24$ L/mol for H^+, $a = 4.32$ Å and $b = 0.06$ L/mol for Na^+, and $a = 3.71$ Å and $b = 0.01$ L/mol for both Cl^- and NO_3^-[69,70].

Finally, I assumed Γ_s^0 had a constant value of 5.7 sites/nm^2. This is based on a assumption of hexagonal ice Ih with an a-axis length of 0.45 nm[71]. With these assumptions and the relationship expressed in Eq. 25, fitting zeta potential versus salinity or pH using Eq. 38 requires optimizing for K_p, K_d, K_C, K_A, and K_{HO}.

III. RESULTS AND DISCUSSION

A. Model predictions

In this section I compare the surface charge model to results in the literature. This comparison involves using measurements of zeta potential as a function of pH and salinity to determine the equilibrium constants and surface charge density by optimizing Eq. 38. In this comparison I assume that the zeta potential is equal to the Stern potential φ_d. While this is not always necessarily the case, in the absence of macromolecule adsorption the two should be very close to each other[60,64]. The literature results I used for this comparison are from Drzymala et al.[33], Kallay et al.[44], and Inagawa et al.[35]. I note here that measuring the zeta potential of the surface of ice in contact with water is difficult. Drzymala et al.[33] used conventional electrophoretic mobility measurements on crushed ice particles in

low-salinity brine, but used D_2O as the ice phase (melting temperature 3.8°C) to allow a working temperature range within which the ice would remain frozen and the brine would remain liquid. Kallay et al.[44] reported the results of Kallay and Čakara[34], who used a specially constructed ice electrode to measure the potential between the ice-coated electrode and the brine solution. Inagawa et al.[35] measured the electrophoretic mobility of tracer particles (polystyrene) in brine through a microchannel in ice and added glycerol to the brine to prevent freezing. The difficulty of making these measurements and the necessity for custom-built equipment means that there are few published results, and that those results can sometimes have large uncertainties (e.g.,[33]).

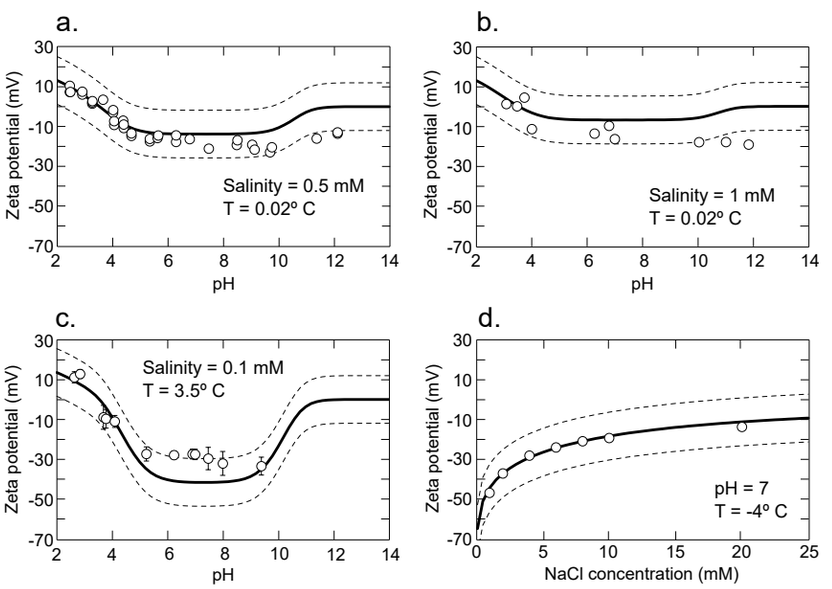

FIG. 2. Comparison of predicted zeta potential from Eq. 38 with literature results. Circles are measured data points, dark black lines are model predictions, and dashed lines are ±2 standard deviations. Salinities and temperatures are noted on each subplot. (a) Data from Kallay and Čakara[34] using water and $NaNO_3$. Zeta potential was measured with an ice electrode. (b) Data from Kallay and Čakara[34] using water and $NaNO_3$. Zeta potential was measured with an ice electrode. (c) Data from Drzymala et al.[33] using frozen D_2O and liquid H_2O with NaCl. Zeta potential was determined from electrophoretic mobility of crushed ice particles in brine solution. (d) Data from Inagawa et al.[35] using water and NaCl with glycerol to prevent freezing. Zeta potential was determined from electrophoretic mobility of polystyrene tracer particles through a microchannel in ice.

The comparison between measurements and predictions from Eq. 38 are shown in Fig. 2. The corresponding equilibrium constants are given in Table 2 with uncertainties determined using the bootstrap method described in Hu et al.[72].

Constant	**Value ± 1 standard deviation**
$\log_{10} K_p$	-0.0617 ± 0.0137
$\log_{10} K_d$	-7.44 ± 1.80
$\log_{10} K_C$	6.45 ± 1.94
$\log_{10} K_A$ (for Cl^-)	0.205 ± 0.0273
$\log_{10} K_A$ (for NO_3^-)	0.160 ± 0.0313
$\log_{10} K_{HO}$	7.60 ± 1.83

TABLE II. Equilibrium constants derived from reported experimental data

Zeta potential values are positive under strongly acidic conditions and negative over the rest of the pH range represented in the data. The pH corresponding to a zeta potential of zero, known as the pH at the point of zero charge or pH(pzc), is the pH value at which $\Gamma^0_{>\mathrm{O}} + \Gamma^0_{\mathrm{O}^-} = \Gamma^0_{\mathrm{OH}_2^+}$. From Eqs. 19, 20, and 23,

$$\mathrm{pH(pzc)} = -\frac{1}{2}\log_{10}\left[\frac{1}{K_p}\left(\frac{1}{K_{HO}} + K_d\right)\right]. \tag{43}$$

Using the average values for K_p, K_d, and K_{HO} from Table 2, I obtain pH(pzc) = 3.69. This is consistent with the results of Drzymala et al.[33] and Kallay et al.[44].

B. Surface site occupancies and surface reactions

The model fits in Fig. 2 all predict that the zeta potential reaches a plateau at pH between about 5 and 10 and decreases to near neutral at pH <11. This behavior can be understood in terms of the number of sites with a given charge present at the ice-water interface. The fractional surface site occupancies are defined in a manner analogous to Eqs. 32 and 33 as

$$\Omega^0_{>\mathrm{O}} = \frac{1}{\alpha K_{HO} a_{\mathrm{H}^+}} \mathrm{e}^{\frac{e\varphi_0}{kT}}, \tag{44}$$

$$\Omega^0_{\mathrm{O}^-} = \frac{K_d}{\alpha a_{\mathrm{H}^+}} \mathrm{e}^{\frac{e\varphi_0}{kT}}, \tag{45}$$

$$\Omega^0_{\mathrm{OH}} = \frac{1}{\alpha}, \tag{46}$$

$$\Omega^0_{\mathrm{OH}_2^+} = \frac{a_{\mathrm{H}^+} K_p}{\alpha} \mathrm{e}^{-\frac{e\varphi_0}{kT}}, \tag{47}$$

$$\Omega^0_{\mathrm{OH_2A}} = \Omega^0_{\mathrm{OH}_2^+} K_A a_{\mathrm{A}^-} \mathrm{e}^{\frac{e\varphi_d}{kT}}, \tag{48}$$

$$\Omega^0_{\mathrm{OC}} = 1 - \Omega^0_{>\mathrm{O}} - \Omega^0_{\mathrm{O}^-} - \Omega^0_{\mathrm{OH}} - \Omega^0_{\mathrm{OH}_2^+} - \Omega^0_{\mathrm{OH_2A}}. \tag{49}$$

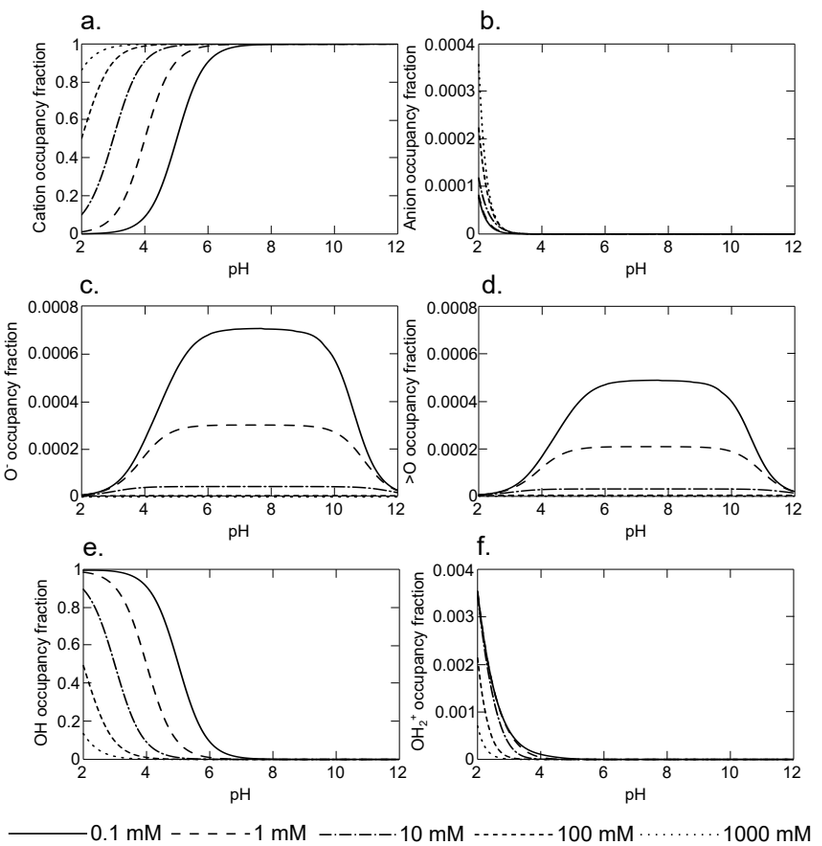

FIG. 3. Fractional site occupancies at different NaCl concentrations at $T = 0°\mathrm{C}$ for cations (a), anions (b), O^- (c), $>\mathrm{O}$ (d), OH (e), and OH_2^+ (f).

Fig. 3 shows $\Omega^0_{>\mathrm{O}}$, $\Omega^0_{\mathrm{O}^-}$, Ω^0_{OH}, $\Omega^0_{\mathrm{OH}_2^+}$, $\Omega^0_{\mathrm{OH_2A}}$, and Ω^0_{OC} as a function of pH at various salinities and $T = 0°\mathrm{C}$ using the average equilibrium constant values from Table 2 (K_A was taken as the value corresponding to Cl^-). While it is not physically possible for ice to exist in

equilibrium with anything except pure water at this temperature, it is useful to perform all the calculations at a consistent temperature. Since adsorption of dissolved ions neutralizes surface charge in the modeled reactions (Eqs. 1–4), any nonzero zeta potential values are due to excess charge that is not neutralized. Therefore, zeta potential should follow the trend of available O^-, $>O$, or OH_2^+ sites. Figs. 3a and 3b show that cations occupy nearly all surface sites above a pH value that decreases as salinity increases, and that anions occupy a small amount of surface sites below pH(pzc). Despite the cation occupancy being so large, some O^- and $>O$ sites are exposed at pH between about 4 and 12, and occupancy of these sites follows the trend of zeta potential (Figs. 3c and 3d). Interestingly, the surface occupancies of cations and OH nearly mirror each other (Fig. 3e).

These features can be explained in terms of the surface reactions assumed in the model (Eqs. 1–6). O^- and $>O$ occupancy are predicted overall to be very small even at low salinity. This suggests that at most only a small fraction of OH sites remain deprotonated, and that $>O$ readily adsorbs cations. On the other hand, the reduction in H^+ concentration in the aqueous phase at elevated pH should drive towards the aqueous phase, so one might expect that O^- and $>O$ should be more abundant on the surface at higher pH. The decrease in O^- and $>O$ surface occupancy at pH >10 appears inconsistent with this, but it is important here to remember my assumption that basic pH is the result of addition of a hydroxide of the aqueous cation (in this case NaOH), which causes the cation concentration in the aqueous phase to increase along with the hydroxide concentration. This would inhibit the preservation of a net negative charge at high pH as any aqueous Na^+ would segregate towards the ice-water interface. The high surface occupancy of Na^+ appears to suggest that nearly all the OH sites deprotonate and that Na^+ replaces the missing H^+ at nearly all of them. This is supported by the complementary relationship between cation and OH occupancies (Figs. 3a and 3e). Inagawa et al.[35] suggested that only about 1.4% of OH sites were deprotonated above pH of 5, which they ascribed to proton disorder of the ice surface inhibiting deprotonation of neighboring OH sites through fast reorientation of water molecules. It is important to note that surface occupancy represents the net concentration on the surface, so these two facts are not necessarily inconsistent. Indeed, the opposite trends of Na^+ and OH occupancy indicate that Na^+ is taking the place of OH on the surface as pH increases, which requires the latter first to be deprotonated. Additional cations are taken up by the $>O$ sites. The small negative zeta potential observed on the ice-water

interface at moderate pH indicates that nearly all of the negative surface sites are neutralized by cations,but the remaining negative surface sites consist of both deprotonated OH and dangling O. It is important to note here that this model does not consider bonding of Na^+ ions with multiple O atoms on the ice surface as suggested, for instance, by the simulations of Shoaib and Choi[42]. This would reduce the number of Na^+ ions required to occupy all available surface sites, but is also inconsistent with the Guoy-Chapman model. A different description of the electrical double layer at the ice-water interface could be developed, but that is beyond the scope of this work.

The computed surface site occupancies in Fig. 3 provide some insight into the relative proportions of dangling OH and dangling O on the ice-water interface. Fletcher[36] suggested that, at low temperatures (<70 K) the ice-air interface contains roughly equal amounts of dangling OH and dangling O. This was supported by Buch et al.[39] using molecular dynamics simulations. On the other hand, Nojima et al.[73] showed that the ice-air interface has predominantly dangling OH at 100 K. Ishiyama and Kitanaka[74] found using molecular dynamics simulations that the ice-water interface contains nearly equal numbers of dangling OH and dangling O, with a slight preference for dangling OH. In Figs. 3c and 3d, the present model predicts that deprotonated OH groups are indeed favored over dangling O, but not by much. From Eqs. 44 and 45, $\frac{\Omega^0_{O^-}}{\Omega^0_{>O}} = \frac{\Gamma^0_{O^-}}{\Gamma^0_{>O}} = K_d K_{HO}$, which means that there are about 1.4 times as many deprotonated OH as there are dangling O, even in pure water. Ishiyama and Kitanaka[74] ascribe this to the fact that more hydrogen bonds exist on average in ice than in water, creating a slight imbalance at the interface. Similar molecular dynamics results were reported by Bryk and Haymet[75]. Overall, my results support these previous results and indicate that the ice-water interface slightly favors dangling OH groups.

C. Surface charge density

The surface charge density Q_s^0 is the sum of the number of each surface site per unit area times its charge (Eq. 26), and is determined as a function of salinity and pH from Eq. 34. The maximum value of Q_s^0 corresponds to complete occupancy of all surface sites either by positive or negative charges and is equal to $\pm e\Gamma_s^0$. Using $\Gamma_s^0 = 5.7$ sites/nm^2 yields a maximum Q_s^0 of ± 0.91 C/m^2. However, because the fractional surface occupancy of different ionic species varies with salinity and pH (Fig. 3), the maximum Q_s^0 may not

necessarily be reached. The value of Q_s^0 is important to constrain as it determines the electrostatic potential of the ice-water interface and electrostatic forces between adjacent ice crystals separated by water, which are significant parameters affecting processes from lightning generation to atmospheric chemistry to frost heave and glacier motion[2,24].

Fig. 4 shows Q_s^0 calculated from Eq. 34 as a function of pH and salinity at 0°C. The average equilibrium constants from Table 2 were used for calculation. For salinities greater than about 100 mM, $Q_s^0 \approx 0$ for pH greater than the point of zero charge (3.69). Q_s^0 is always positive for pH < 3.69, and negative for pH > 3.69 at lower salinities. However, Q_s^0 remains well below the maximum value in the range of pH and salinity I considered. This broadly follows the trends of the unoccupied positive and negative surface sites (Fig. 3), driven by the strong affinity of Na^+ for the surface at alkaline pH and the abundance of exposed neutral surface sites at acidic pH.

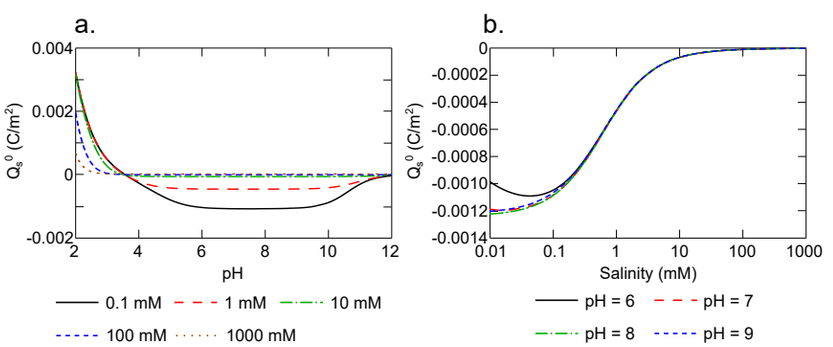

FIG. 4. Surface charge density at $T = 0$°C as a function of pH (a) and salinity (b).

These surface charge density values have implications for the thickness of a premelted layer that can exist between ice grains or between ice and air. Wettlaufer[10] presented an analysis of the equilibrium premelted layer thickness by minimizing the total system free energy, including excess surface energy contributed by van der Waals and electrostatic interactions. The equilibrium premelted layer thickness therefore depends on a balance of colligative, van der Waals, and electrostatic energies. Thomson et al.[76] compared this theory with optical measurements of premelted layer thickness at ice grain boundaries in equilibrium with brines of varying salinity, and showed that the results could be explained by the limit in which electrostatic repulsion was insignificant (i.e., small Q_s^0), though they also showed that the data could equally be explained by assuming a very large Q_s^0. For $|Q_s^0| \sim \mathcal{O}(10^{-3})$ C/m^2, model-based calculations of premelted layer thickness indicate that

the thickness scales inversely with undercooling for NaCl concentrations above about 1 mM[77], which suggests that electrostatic repulsion is negligible above this salinity with the surface charge densities I predicted. The calculated layer thicknesses are < 10 nm for undercoolings larger than about 0.1 K. That being said, model calculations are sensitive to input parameters that may have considerable uncertainty, for example Hamaker constants. In their recent review on premelting, Slater and Michaelides[78] present a summary of physical measurements of premelted layer thickness as a function of temperature, which indicates that the layer is generally thinner than 10 nm, and persist to temperatures as low as about 248 K. This is consistent with the simulation results of Llombart et al.[22]. Since larger surface charge densities tend to cause the premelted layer to collapse at larger temperatures[77], my results are consistent with the general idea of the ice-water interface having a sufficiently low surface charge density that premelted layer thickness is governed mainly by van der Waals and colligative energies.

D. Partitioning of cations in the electrical double layer and induced polarization

The cations in the electrical double layer will be partitioned between the diffuse and Stern layers. Understanding the degree of this partitioning is important for predicting the electrical properties of the ice-water interface, and particularly the frequency dependence of those properties. In the presence of an alternating electrical field, the complex conductivity of porous media such as sand packs and glass beads exhibits exhibit an increase in the imaginary (quadrature) component of conductivity at low frequencies (<100 Hz). This relaxation is generally attributed to polarization of the Stern and/or diffuse layers, which occurs as charges move within the electrical double layer in response to the applied external field. Stern and diffuse layer polarization has been studied extensively by many authors[79–87], and it is not relevant here for me to describe the phenomena in detail. I note here that I focus in this section on induced polarization due to ionic mobility in the electrical double layer. Several other polarization mechanisms operate at the ice-water interface, including rotational relaxations in the ice and water near the ice surface caused by the intrinsic dipole of water[88,89]. These effects at higher frequency could be accounted for through consideration of the orientation of water molecules that associate with the OH and dangling O surface

sites, but that is beyond the scope of the present study.

Generally speaking, the amount of polarization that occurs in the Stern and diffuse layers and the corresponding imaginary conductivity response depends on the concentration of ions within each layer and their mobilities[85,87]. Complex conductivity measurements of sand packs, glass beads, and clays show evidence of this polarization, even in materials with low surface area[90]. In contrast, when complex conductivity measurements are performed on mixtures of sediments, ice, and brine, there is no apparent contribution from polarization of the electrical double layer at the ice-water interface, with only the electrical double layer on the mineral grains affecting the response[8,89,91]. A large body of literature on the electrical conductivity of ice (both low-frequency and high-frequency) similarly suggests that the electrical double layer at the ice-water interface plays little to no role in electrical conduction, and that the conductivity of brine channels at grain boundaries follows Archie's law with no contribution from conduction in the electrical double layer[53,88,89,92–95]. These measurements suggest instead that Jaccard theory[96] best describes electrical conductivity of ice, whereby current flows via migration of proton point defects, even at the ice-water interface[89].

The apparent lack of Stern and diffuse layer polarization and contribution of the electrical double layer to ice conductivity can be explained in terms of the charge distribution within the electrical double layer. Following Leroy et al.[85,97], I define a partition coefficient f for the counterions, which is the fraction of counterions in the electrical double layer that are contained in the Stern layer:

$$f = \frac{\Gamma_i^0}{\Gamma_i^0 + \Gamma_i^d}, \tag{50}$$

where Γ_i^d is the equivalent surface site density in the diffuse layer. Since the counterions are cations at pH > pH(pzc) and anions at pH < pH(pzc), the subscript i can refer either to cations or anions depending on pH. The equivalent site densities are defined as

$$\Gamma_i^d \equiv 1000 N_A C_i^f \int_0^{\frac{2}{\kappa}} (\exp[-\frac{z_i e \varphi(x)}{kT} - 1]) \, \mathrm{d}x, \tag{51}$$

where $\varphi(x)$ is the local potential at a distance x from the ice-water interface[59,97]. Using the Debye-Hückel approximation,

$$\varphi(x) \approx \varphi_d \exp(-\kappa x). \tag{52}$$

The surface site densities are $\Gamma^0_{\mathrm{OH_2A}} = \Gamma^0_s \Omega^0_{\mathrm{OH_2A}}$ and $\Gamma^0_{\mathrm{OC}} = \Gamma^0_s \Omega^0_{\mathrm{OC}}$, where Ω^0_{OC} and $\Omega^0_{\mathrm{OH_2A}}$ are given by Eqs. 48 and 49.

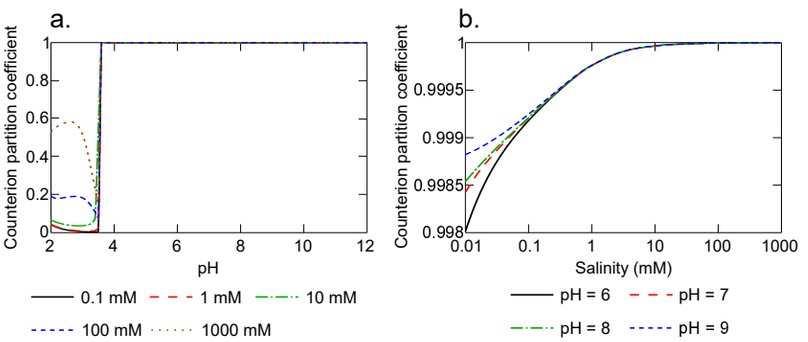

FIG. 5. Counterion partition coefficient as a function of pH (a) and salinity (b) at $T = 0°\mathrm{C}$. Note that for pH < pH(pzc), the counterions are anions, while for pH > pH(pzc) the counterions are cations.

Fig. 5 shows the partition coefficient as a function of pH and salinity at 0°C. For pH > pH(pzc), almost all the counterions are contained in the Stern layer, while at pH < pH(pzc) partitioning is more variable. In the pH range of 6–9, which is of greatest interest for geophysical and atmospheric applications, $f > 0.998$ over the entire salinity range I considered. This indicates that nearly all the counterions are contained in the Stern layer and that the ion concentration in the diffuse layer is nearly identical to that of the bulk aqueous phase. There are two main implications arising from this result. First, there is very little excess conductivity in the diffuse layer with respect to the bulk electrolyte, and regardless of salinity the electrical double layer will behave as if the diffuse layer had negligible thickness. Overall this means that no diffuse layer polarization will occur and that the diffuse layer does not contribute to excess surface conductivity. This is consistent with observations. Second, the high concentration of counterions in the Stern layer is likely related to the observed lack of Stern layer conductivity and polarization due to reduced counterion mobility. Some clays, particularly kaolinite, have similarly large proportions of counterions in their Stern layers ($f > 0.95$)[98] and the dense packing of counterions appears to result in a drastically reduced mobility within the Stern layer (at least 100 times smaller)[86]. It is not surprising therefore that the ice-water interface has a negligible conductivity contribution from the electrical double layer and exhibits little low-frequency relaxation response. The fact that counterions can penetrate partially into the ice surface will additionally restrict

their mobility.

IV. CONCLUSIONS

The hypothesis underlying this work was that existing models for describing the electrical double layer at metal oxide-water interfaces should be able to be modified to describe the surface charge, surface potential, and ionic occupancy at the ice-water interface. To test this, I used an existing model for the electrical double layer at metal oxide-brine interfaces to describe the surface charge and ion occupancy at the ice-water interface. The model considers protonation and deprotonation on the ice surface as well as adsorption of aqueous ions. I compared the model to measurements of ice zeta potential in brines of various strengths and pH to determine the equilibrium constants for each of the surface reactions. The results indicated a consistent pH at the point of zero charge of 3.69. Aqueous cation adsorption is by far the dominant surface reaction, even at very low salinities, with an equilibrium constant at least 5 orders of magnitude larger than the others. These cations occupy nearly all the available surface sites at pH > 7 in fresh water (0.1 mM salinity) and at pH > 3 in brines of seawater salinity or higher. Deprotonated OH groups are slightly favored over dangling O sites, which is consistent with previous work[74,75]. At moderate pH (between 6 and 9), the surface charge density varies from around -0.001 C/m^2 at salinity < 1 mM to near 0 at higher salinity.

The surface complexation model allowed me to make predictions about the partitioning of counterions between the Stern and diffuse layers. For pH < 3.69, the counterions are anions and are preferentially located in the diffuse layer. However, when pH > 3.69 and the counterions are cations, the partition coefficient is > 0.998, indicating that the vast majority of the counterions are located in the Stern layer. This has important implications for electrical conductivity and the induced polarization response of the ice-water interface at the moderate pH values of interest to atmospheric and geophysical applications. In particular, diffuse layer polarization will not occur since the ionic concentration in the diffuse layer is nearly identical to that of the bulk electrolyte, and Stern layer polarization and electrical conduction will tend not to occur because the high cation concentration and partial penetration into the ice surface will drastically reduce cation mobility. This is consistent with observations.

ACKNOWLEDGMENTS

Two anonymous reviewers provided comments that greatly strengthened this paper. Thanks to Alan Rempel for helpful comments on this manuscript and for pointing me in the direction of the literature on electrical conductivity of polar ice and ice cores. This work was supported by the University of Texas at Austin, and the Laboratory Directed Research and Development program at Sandia National Laboratories. Sandia National Laboratories is a multimission laboratory managed and operated by National Technology and Engineering Solutions of Sandia, LLC., a wholly owned subsidiary of Honeywell International, Inc., for the U.S. Department of Energy's National Nuclear Security Administration under contract DE-NA-0003525.

DATA AVAILABILITY STATEMENT

Data sharing is not applicable to this article as no new data were created or analyzed in this study.

REFERENCES

[1]V. Petrenko and R. Whitworth, *Physics of ice* (Oxford University Press, 1999).

[2]J. Dash, A. Rempel, and J. Wettlaufer, "The physics of premelted ice and its geophysical consequences," Reviews of Modern Physics **78**, 695–741 (2006).

[3]D. Vonder Mühll, C. Hauck, and H. Gubler, "Mapping of mountain permafrost using geophysical methods," Progress in Physical Geography: Earth and Environment **26**, 643–660 (2002).

[4]C. Hauck, K. Isaksen, D. Vonder Mühll, and J. Sollid, "Geophysical surveys designed to delineate the altitudinal limit of mountain permafrost: an example from Jotunheimen," Permafrost and Periglacial Processes **15**, 191–205 (2004).

[5]C. Kneisel, C. Hauck, R. Fortier, and B. Moorman, "Advances in geophysical methods for permafrost investigations," Permafrost and Periglacial Processes **19**, 157–178 (2008).

[6]D. Sherman and S. Constable, "Permafrost extent on the Alaskan Beaufort Shelf from surface-towed controlled-source electromagnetic surveys," Journal of Geophysical Research Solid Earth **123**, 7253–7265 (2018).

[7]S. Springman, Y. Yamamoto, T. Buchli, M. Hertrich, H. Maurer, K. Merz, I. Gärtner-Roer, and L. Seward, "Rock glacier degradation and instabilities in the european alps: a characterisation and monitoring experiment in the turtmanntal, ch," in *Landslide science and practice*, edited by C. Margottini, P. Canuti, and K. Sassa (Springer, 2013) pp. 5–13.

[8]P. Duvillard, A. Revil, Y. Qi, A. Soueid Ahmed, A. Coperey, and L. Ravanel, "Three-dimensional electrical conductivity and induced polarization tomography of a rock glacier," Journal of Geophysical Research Solid Earth **123**, 9528–9554 (2018).

[9]J. Caranti and A. Illingworth, "Frequency dependence of the surface conductivity of ice," The Journal of Physical Chemistry **87**, 4078–4083 (1983).

[10]J. Wettlaufer, "Impurity effects in the premelting of ice," Physical Review Letters **82**, 2516–2519 (1999).

[11]E. Kuiper, J. de Bresser, M. Drury, J. Eichler, G. Pennock, and I. Weikusat, "Using a composite flow law to model deformation in the NEEM deep ice core, Greenland – Part 2: The role of grain size and premelting on ice deformation at high homologous temperature," The Cryosphere **14**, 2449–2467 (2020).

[12]M. Leu, S. Moore, and L. Keyser, "Heterogeneous reactions of chlorine nitrate and hydrogen chloride on type I polar stratospheric clouds," The Journal of Physical Chemistry **95**, 7763–7771 (1991).

[13]M. Molina, R. Zhang, P. Wooldridge, J. McMahon, J. Kim, H. Chang, and K. Beyer, "Physical chemistry of the $H_2SO_4/HNO_3/H_2O$ system: implications for polar stratospheric clouds," Science **261**, 1418–1423 (1993).

[14]A. Tabazadeh and R. Turco, "A model for heterogeneous chemical processes on the surfaces of ice and nitric acid trihydrate particles," Journal of Geophysical Research Atmospheres **98**, 12727–12740 (1993).

[15]L. Pauling, "The structure and entropy of ice and of other crystals with some randomness of atomic arrangement," Journal of the American Chemical Society **57**, 2680–2684 (1935).

[16]M. Shultz, "Ice surfaces," Annual Review of Physical Chemistry **68**, 285–304 (2017).

[17]V. Petrenko, "The surface of ice," Tech. Rep. Special Report 94-22, Cold Regions Research & Engineering Laboratory, Hanover, N.H. (1994).

[18]N. Fletcher, "Surface structure of water and ice," Philosophical Magazine **7**, 255–269 (1962).

[19]N. Fletcher, "Surface structure of water and ice — a reply and a correction," Philosophical Magazine B **8**, 1425–1426 (1963).

[20]V. Petrenko and S. Colbeck, "Generation of electric fields by ice and snow friction," Journal of Applied Physics **77**, 4518–4521 (1995).

[21]H. Dosch, A. Lied, and J. Bilgram, "Disruption of the hydrogen-bonding network at the surface of Ih ice near surface premelting," Surface Science **366**, 43–50 (1996).

[22]P. Llombart, E. Noya, and L. MacDowell, "Surface phase transitions and crystal habits of ice in the atmosphere," Science Advances **6**, eaay9322 (2020).

[23]T. Takahashi, "Riming electrification as a charge generation mechanism in thunderstorms," Journal of the Atmospheric Sciences **35**, 1536–1548 (1978).

[24]J. Dash and J. Wettlaufer, "The surface physics of ice in thunderstorms," Canadian Journal of Physics **81**, 201–207 (2003).

[25]P. Jungwirth, D. Rosenfeld, and V. Buch, "A possible new molecular mechanism of thundercloud electrification," Atmospheric Research **76**, 190–205 (2005).

[26]A. Pedersen, K. Wikfeldt, L. Karssemeijer, H. Cuppen, and H. Jónsson, "Molecular reordering processes on ice (0001) surface from long timescale simulations," The Journal of Chemical Physics **141**, 234706 (2014).

[27]J. Dash, B. Mason, and J. Wettlaufer, "Theory of charge and mass transfer in ice-ice collisions," Journal of Geophysical Research Atmospheres **106**, 20395–20402 (2001).

[28]H. Hansen-Goos and J. Wettlaufer, "Theory of ice premelting in porous media," Physical Review E **81**, 031604 (2010).

[29]P. Leroy, D. Jougnot, A. Revil, A. Lassin, and M. Azaroual, "A double layer model of the gas bubble/water interface," Journal of Colloid and Interface Science **388**, 243–256 (2012).

[30]N. Kallay, T. Preočanin, A. Selmani, D. Kovačević, J. Lützenkirchen, H. Nakahara, and O. Shibata, "Thermodynamic model of charging the gas/water interface," The Journal of Physical Chemistry C **119**, 997–1007 (2019).

[31]E. Nechaev and I. Ivanov, "The electric double layer at the ice-electrolyte interface," Kolloidnyi Zhurnal **36**, 583–584 (1974).

[32]E. Nechaev, V. Romanov, and T. Golovanova, "Mobility of ions of electric double-layer at alumina-electrolyte interface," Kolloidnyi Zhurnal **37**, 57–61 (1975).

[33]J. Drzymala, Z. Sadowski, L. Holysz, and E. Chibowski, "Ice/water interface: zeta potential, point of zero charge, and hydrophobicity," Journal of Colloid and Interface Science **220**, 229–234 (1999).

[34]N. Kallay and D. Čakara, "Reversible charging of the ice-water interface: I. Measurement of the surface potential," Journal of Colloid and Interface Science **232**, 81–85 (2000).

[35]A. Inagawa, M. Harada, and T. Okada, "Charging of the ice/solution interface by deprotonation of dangling bonds, ion adsorption, and ion uptake in an ice crystal as revealed by zeta potential determination," The Journal of Physical Chemistry C **123**, 6062–6069 (2019).

[36]N. Fletcher, "Reconstruction of ice crystal surfaces at low temperatures," Philosophical Magazine B **66**, 109–115 (1992).

[37]N. Materer, U. Starke, A. Barbieri, M. Van Hove, G. Somorjai, G. Kroes, and C. Minot, "Molecular surface structure of a low-temperature ice Ih(0001) crystal," The Journal of Physical Chemistry **99**, 6267–6269 (1995).

[38]G. Bussolin, S. Casassa, C. Pisani, and P. Ugliengo, "*Ab initio* study of HCl and HF interaction with crystalline ice. I. Physical adsorption," The Journal of Chemical Physics **108**, 9516–9528 (1998).

[39]V. Buch, H. Groenzin, I. Li, M. Shultz, and E. Tosatti, "Proton order in the ice crystal surface," Proceedings of the National Academy of Science of the United States of America **105**, 5969–5974 (2008).

[40]D. Pan, L. Liu, G. Tribello, B. Slater, A. Michaelides, and E. Wang, "Surface energy and surface proton order of ice Ih," Physical Review Letters **101**, 155703 (2008).

[41]A. Lee and S. Rick, "Characterizing charge transfer at water ice interfaces," The Journal of Physical Chemistry Letters **3**, 3199–3203 (2012).

[42]M. Shoaib and C. Choi, "Na^+, F^-, Br^-, and Cl^- adsorptions and penetrations on an ice surface," ACS Earth and Space Chemistry **2**, 56–63 (2018).

[43]V. Petrenko and I. Ryzhkin, "Surface states of charge carriers and electrical properties of the surface layer of ice," The Journal of Physical Chemistry B **101**, 6285–6289 (1997).

[44]N. Kallay, A. Čop, E. Chibowski, and L. Holysz, "Reversible charging of the ice-water interface II. Estimation of equilibrium parameters," Journal of Colloid and Interface Science **259**, 89–96 (2003).

[45]J. Bernal and R. Fowler, "A theory of water and ionic solution, with particular reference to hydrogen and hydroxyl ions," The Journal of Chemical Physics **1**, 515–548 (1933).

[46]N. Bjerrum, "Structure and properties of ice," Science **115**, 385–390 (1952).

[47]Z. Sun, D. Pan, L. Xu, and E. Wang, "Role of proton ordering in adsorption preference of polar molecule on ice surface," Proceedings of the National Academy of Science of the United States of America **109**, 13177–13181 (2012).

[48]D. Pan, L. Liu, G. Tribello, B. Slater, A. Michaelides, and E. Wang, "Surface energy and surface proton order of the ice Ih basal and prism surfaces," Journal of Physics: Condensed Matter **22**, 074209 (2010).

[49]J. Hayward and A. Haymet, "The ice/water interface: Molecular dynamics simulations of the basal, prism, $20\bar{2}1$, and $2\bar{1}\bar{1}0$ interfaces of ice Ih," The Journal of Chemical Physics **114**, 3713–3726 (2001).

[50]J. Hayward and A. Haymet, "The ice/water interface: orientational order parameters for the basal, prism, $20\overline{2}1$, and $2\bar{1}\bar{1}0$ interfaces of ice Ih," Physical Chemistry Chemical Physics **4**, 3712–3719 (2002).

[51]E. Smith, T. Bryk, and A. Haymet, "Free energy solvation of simple ions: Molecular-dynamics study of solvation of Cl^- and Na^+ in the ice/water interface," The Journal of Chemical Physics **123**, 034706 (2005).

[52]A. Haymet, T. Bryk, and E. Smith, "Solute ions at ice/water interface," in *Ionic soft matter: Modern trends in theory and applications*, edited by D. Henderson, M. Holovko, and A. Trokhymchuk (Springer, 2005) pp. 333–359.

[53]D. Stillman, J. MacGregor, and R. Grimm, "The role of acids in electrical conduction through ice," Journal of Geophysical Research Earth Surface **118**, 1–16 (2013).

[54]M. Conde, M. Rovere, and P. Gallo, "Spontaneous NaCl-doped ice at seawater conditions: focus on the mechanisms of ion inclusion," Physical Chemistry Chemical Physics **19**, 9566–9574 (2017).

[55]Y. Yi, Y. Han, S. Lee, and S. Hur, "Atomistic view of mercury cycling in polar snowpacks: probing the role of Hg^{2+} adsorption using ab initio calculations," Minerals **9**, 459 (2019).

[56]J. Westall, "Adsorption mechanisms in aquatic surface chemistry," in *Aquatic surface chemistry*, edited by W. Stumm (John Wiley & Sons, 1987) pp. 3–32.

[57]P. Schindler and W. Stumm, "The surface chemistry of oxides, hydroxides, and oxide minerals," in *Aquatic surface chemistry*, edited by W. Stumm (John Wiley & Sons, 1987)

pp. 83–110.

[58]D. Grahame, "The electrical double layer and the theory of electrocapillarity," Chemical Reviews **41**, 441–501 (1947).

[59]A. Revil and P. Glover, "Theory of ionic-surface electrical conduction in porous media," Physical Review B **55**, 1757–1773 (1997).

[60]S. Pride, "Governing equations for the coupled electromagnetics and acoustics of porous media," Physical Review B **50**, 15678–15696 (1994).

[61]P. Hesleitner, N. Kallay, and E. Matijević, "Adsorption at solid/liquid interfaces. 6. the effect of methanol and ethanol on the ionic equilibria at the hematite/water interface," Langmuir **7**, 178–184 (1991).

[62]D. Kovačević, I. Kobal, and N. Kallay, "Adsorption of organic acids on metal oxides. the umbrella effect," Croatia Chemica Acta **71**, 1139–1153 (1998).

[63]A. Revil and P. Glover, "Nature of surface electrical conductivity in natural sands, sandstones, and clays," Geophysical Research Letters **25**, 691–694 (1998).

[64]J. Berg, *An introduction to interfaces & colloids* (World Scientific, 2010).

[65]J. Lyklema, *Fundamentals of interface and colloid science: Volume II: Solid-liquid interfaces* (Academic Press, 1995).

[66]D. Yates, S. Levine, and T. Healy, "Site-binding model of the electrical double layer at the oxide/water interface," Journal of the Chemical Society, Faraday Transactions 1 **70**, 1807–1818 (1974).

[67]M. Blesa and N. Kallay, "The metal oxide – electrolyte solution interface revisited," Advances in Colloid and Interface Science **28**, 111–134 (1988).

[68]R. Robinson and R. Stokes, *Electrolyte solutions, 2nd ed.* (Butterworths Scientific Publications, 1959).

[69]D. Parkhurst, "Ion-association models and mean activity coefficients of various salts," in *Chemical modeling of aqueous systems II*, edited by D. Melchior and R. Bassett (American Chemical Society, 1990) pp. 30–43.

[70]J. Kielland, "Individual activity coefficients of ions in aqueous solutions," Journal of the American Chemical Society **59**, 1675–1678 (1937).

[71]A. Fortes, "Accurate and precise lattice parameters of H_2O and D_2O ice Ih between 1.6 and 270 K from high-resolution time-of-flight neutron powder diffraction data," Acta Crystallographica B **B74**, 196–216 (2018).

[72]W. Hu, J. Xie, H. Chau, and B. Si, "Evaluation of parameter uncertainties in nonlinear regression using Microsoft Excel spreadsheet," Environmental Systems Research **4**, 4 (2015).

[73]Y. Nojima, Y. Shioya, H. Torii, and S. Yamaguchi, "Hydrogen order at the surface of ice Ih revealed by vibrational spectroscopy," Chemical Communications **56**, 4563–4566 (2020).

[74]T. Ishiyama and K. Kitanaka, "Asymmetric hydrogen-bonding structure at a water/ice interface," The Journal of Physical Chemistry C **124**, 23287–23294 (2020).

[75]T. Bryk and A. Haymet, "Ice Ih/water interface of the SPC/E model: Molecular dynamics simulations of the equilibrium basal and prism interfaces," The Journal of Chemical Physics **117**, 10258–10268 (2002).

[76]E. Thomson, H. Hansen-Goos, J. Wettlaufer, and L. Wilen, "Grain boundary melting in ice," The Journal of Chemical Physics **138**, 124707 (2013).

[77]L. Benatov and J. Wettlaufer, "Abrupt grain boundary melting in ice," Physical Review E **70**, 061606 (2004).

[78]B. Slater and A. Michaelides, "Surface premelting of water ice," Nature Reviews Chemistry **3**, 179–188 (2019).

[79]G. Schwarz, "A theory of the low-frequency dielectric dispersion of colloidal particles in electrolyte solution," The Journal of Physical Chemistry **66**, 2636–2642 (1962).

[80]J. Schurr, "On the theory of the dielectric dispersion of spherical colloidal particles in electrolyte solution," The Journal of Physical Chemistry **68**, 2407–2413 (1964).

[81]S. Dukhin and V. Shilov, *Dielectric phenomena and the double layer in disperse systems and polyelectrolytes* (John Wiley & Sons, 1974).

[82]O. de Lima and M. Sharma, "A generalized Maxwell-Wagner theory for membrane polarization in shaly sands," Geophysics **57**, 431–440 (1992).

[83]D. Lesmes and F. Morgan, "Dielectric spectroscopy of sedimentary rocks," Journal of Geophysical Research Solid Earth **106**, 13329–13346 (2001).

[84]V. Shilov, A. Delgado, F. Gonzalez-Caballero, and C. Grosse, "Thin double layer theory of the wide-frequency range dielectric dispersion of suspensions of non-conducting spherical particles including surface conductivity of the stagnant layer," Colloids and Surfaces A **192**, 253–265 (2001).

[85]P. Leroy, A. Revil, A. Kemna, P. Cosenza, and A. Ghorbani, "Complex conductivity of water-saturated packs of glass beads," Journal of Colloid and Interface Science **321**, 103–117 (2008).

[86]A. Revil, "Spectral induced polarization of shaly sands: Influence of the electrical double layer," Water Resources Research **48**, W02517 (2012).

[87]M. Bücker, A. Flores Orozco, S. Undorf, and A. Kemna, "On the role of stern- and diffuse-layer polarization mechanisms in porous media," Journal of Geophysical Research Solid Earth **124**, 5656–5677 (2019).

[88]R. Grimm, D. Stillman, S. Dec, and M. Bullock, "Low-frequency electrical properties of polycrystalline saline ice and salt hydrates," The Journal of Physical Chemistry B **112**, 15382–15390 (2008).

[89]D. Stillman, R. Grimm, and S. Dec, "Low-frequency electrical properties of ice-silicate mixtures," The Journal of Physical Chemistry B **114**, 6065–6073 (2010).

[90]A. Revil and N. Florsch, "Determination of permeability from spectral induced polarization in granular media," Geophysical Journal International **181**, 1480–1498 (2010).

[91]A. Coperey, A. Revil, F. Abdulsamad, B. Stutz, P. Duvillard, and L. Ravanel, "Low-frequency induced polarization of porous media undergoing freezing: Preliminary observations and modeling," Journal of Geophysical Research Solid Earth **124**, 4523–4544 (2019).

[92]E. Wolff and J. Paren, "A two-phase model of electrical conduction in polar ice sheets," Journal of Geophysical Research Solid Earth **89**, 9433–9438 (1984).

[93]J. Moore, J. Paren, and H. Oerter, "Sea salt dependent electrical conduction in polar ice," Journal of Geophysical Research Solid Earth **97**, 19803–19812 (1992).

[94]J. Moore, A. Reid, and J. Kipfstuhl, "Microstructure and electrical properties of marine ice and its relationship to meteoric ice and sea ice," Journal of Geophysical Research Oceans **99**, 5171–5180 (1994).

[95]E. Wolff, W. Miners, J. Moore, and J. Paren, "Factors controlling the electrical conductivity of ice from the polar regions – A summary," The Journal of Physical Chemistry B **101**, 6090–6094 (1997).

[96]C. Jaccard, "Thermodynamics of irreversible processes applied to ice," Physik der Kondensierten Materie **3**, 99–118 (1964).

[97]P. Leroy, A. Revil, S. Altmann, and C. Tournassat, "Modeling the composition of pore water in a clay-rock geological formation (Callovo-Oxfordian, France)," Geochimica et

Cosmochimica Acta **71**, 1087–1097 (2007).

[98]P. Leroy and A. Revil, "A mechanistic model for the spectral induced polarization of clay materials," Journal of Geophysical Research Solid Earth **114**, B10202 (2009).

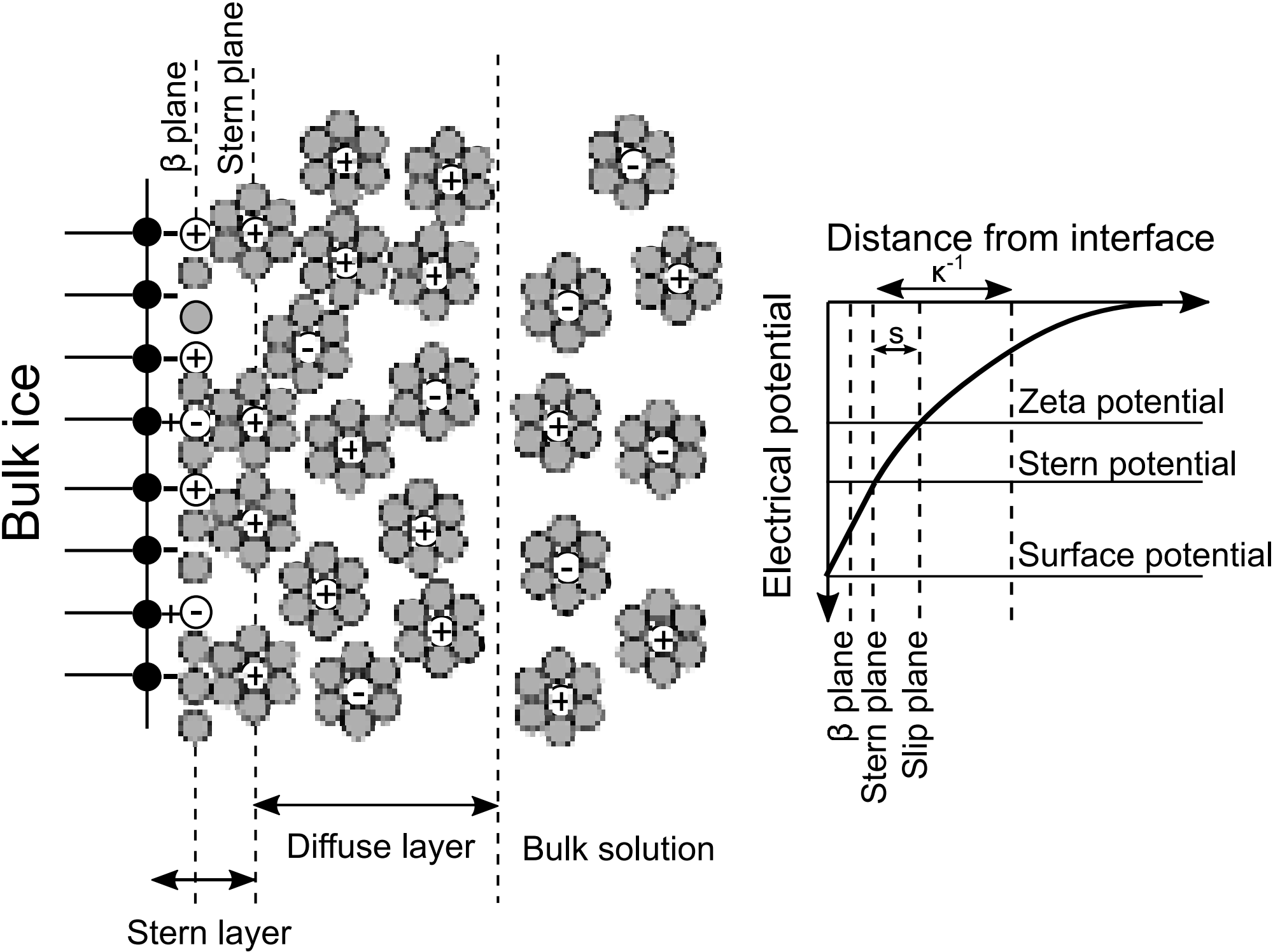
Bulk ice
β plane
Stern plane
Diffuse layer
Bulk solution
Stern layer
Distance from interface
Electrical potential
κ-1
s
Zeta potential
Stern potential
Surface potential
β plane
Stern plane
Slip plane

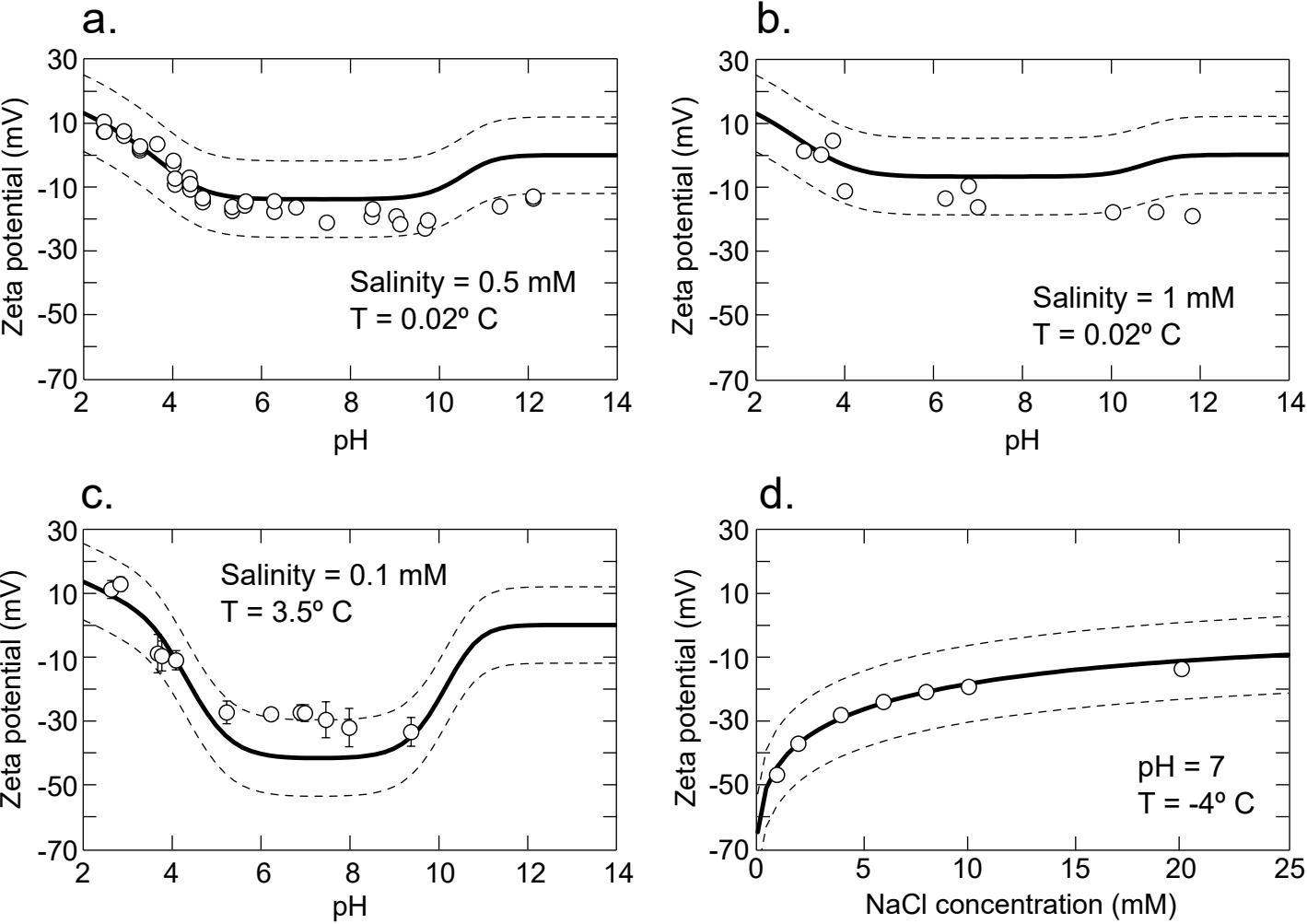
a.
Zeta potential (mV)
30
10
-10
-30
-50
-70
2
4
6
8
10
12
14
pH
Salinity = 0.5 mM
T = 0.02º C
b.
Zeta potential (mV)
pH
Salinity = 1 mM
T = 0.02º C
c.
Zeta potential (mV)
pH
Salinity = 0.1 mM
T = 3.5º C
d.
Zeta potential (mV)
0
5
10
15
20
25
NaCl concentration (mM)
pH = 7
T = -4º C

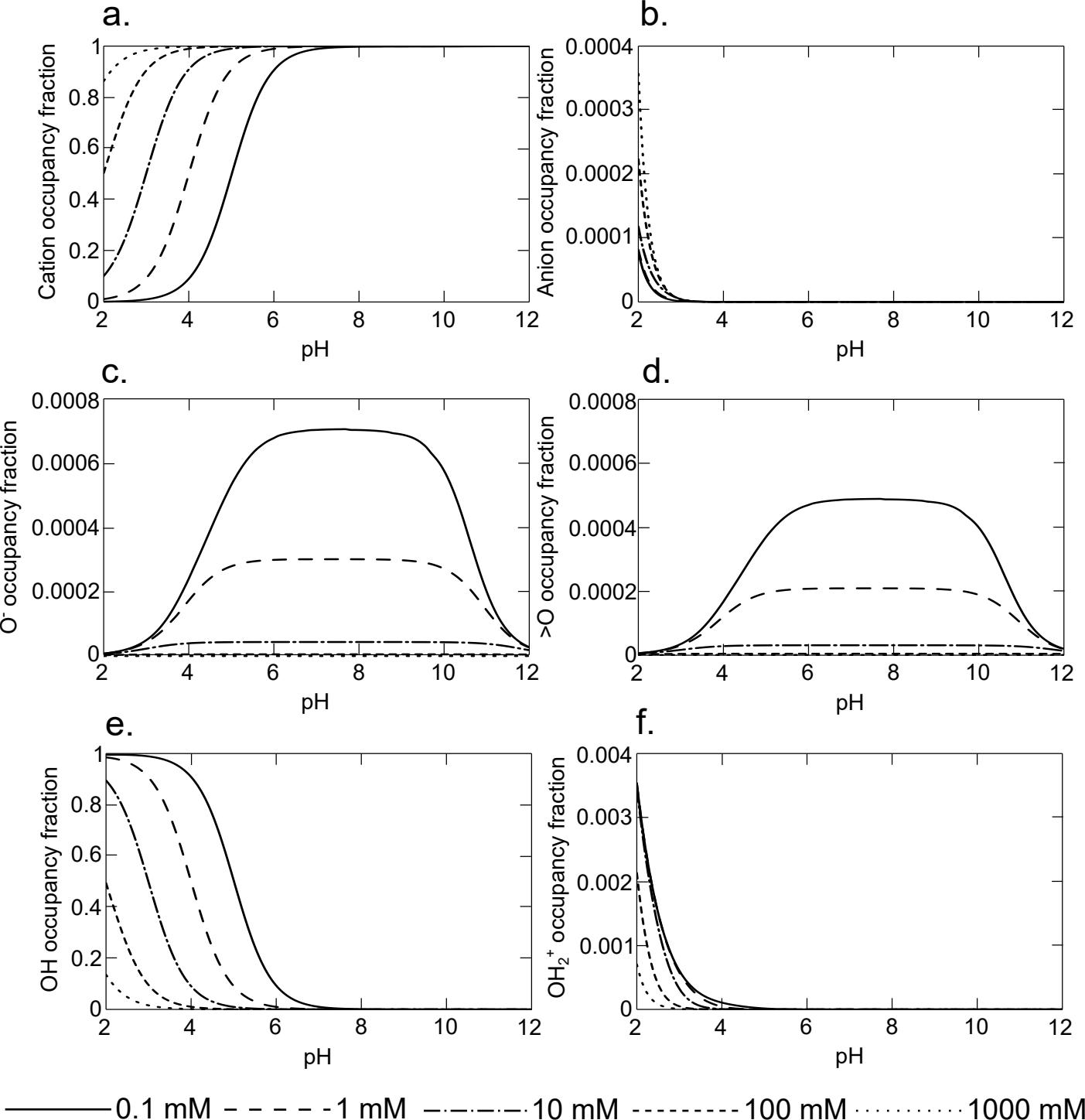
a.
b.
c.
d.
e.
f.
Cation occupancy fraction
Anion occupancy fraction
O⁻ occupancy fraction
>O occupancy fraction
OH occupancy fraction
OH2+ occupancy fraction
pH
0.1 mM
1 mM
10 mM
100 mM
1000 mM

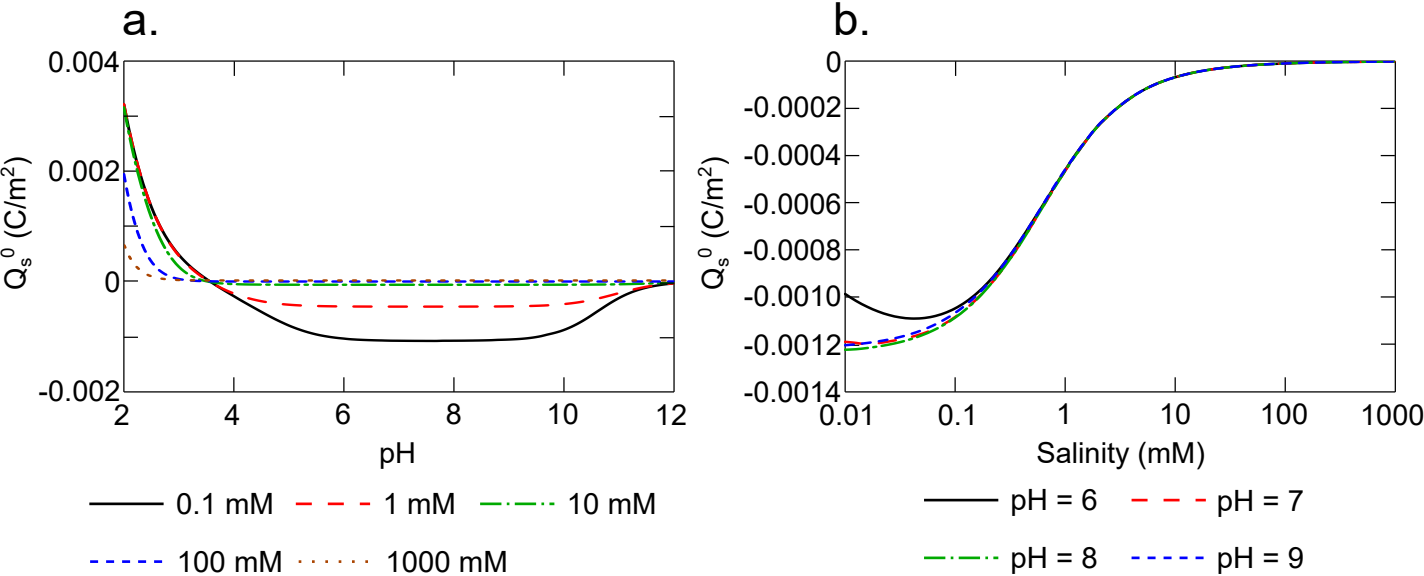
a.
b.
0.004
0.002
0
-0.002
Q_s^0 (C/m^2)
2
4
6
8
10
12
pH
0.1 mM
1 mM
10 mM
100 mM
1000 mM
0
-0.0002
-0.0004
-0.0006
-0.0008
-0.0010
-0.0012
-0.0014
0.01
0.1
1
10
100
1000
Salinity (mM)
pH = 6
pH = 7
pH = 8
pH = 9

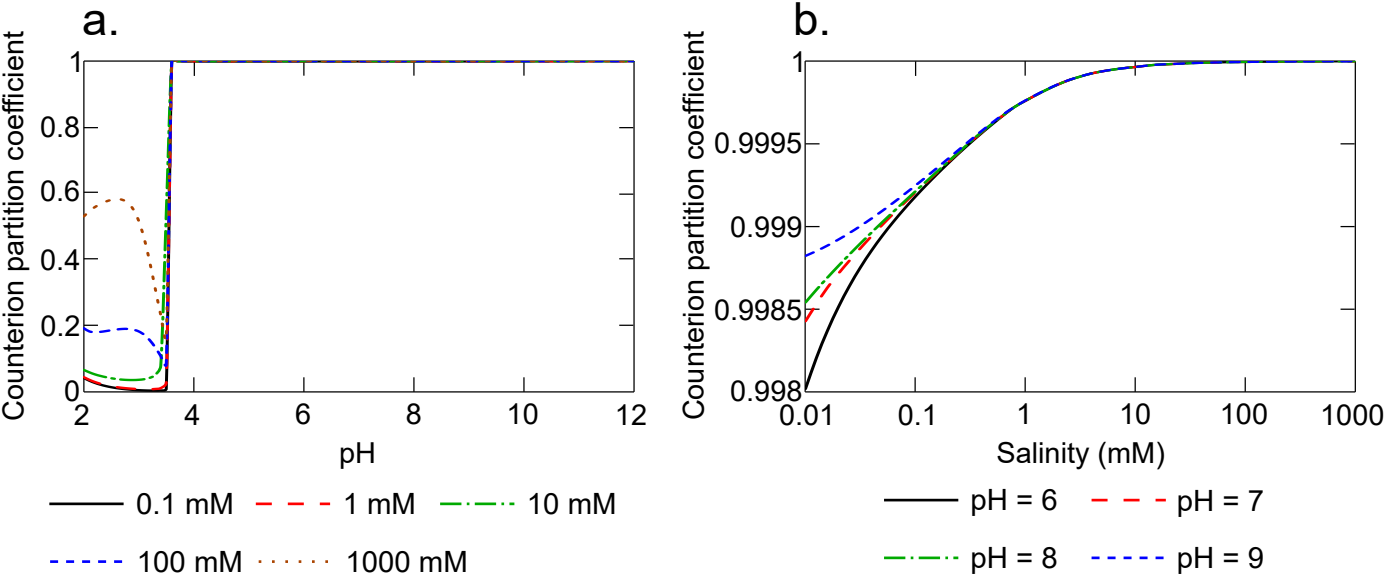
a.
Counterion partition coefficient
1
0.8
0.6
0.4
0.2
0
2
4
6
8
10
12
pH
0.1 mM
1 mM
10 mM
100 mM
1000 mM
b.
Counterion partition coefficient
1
0.9995
0.999
0.9985
0.998
0.01
0.1
1
10
100
1000
Salinity (mM)
pH = 6
pH = 7
pH = 8
pH = 9